

Red Organic Light-Emitting-Diodes based on a N-Annulated Perylene Diimide Dimer

Sergey V. Dayneko,^a Mohammad Rahmati,^b Majid Pahlevani,^{c,} Gregory C. Welch^{a,*}*

^aDepartment of Chemistry, University of Calgary, 731 Campus Place NW, Calgary, Alberta, Canada T2N 1N4

^bGenoptic LED Inc, 6000 72nd Ave SE, Calgary, AB, Canada, T2C 5B1

^cDepartment of Electrical and Computer Engineering, Queen's University, 19 Union St., Kingston, ON, Canada, K7L 3N6

*E-mail: majid.pahlevani@queensu.ca and gregory.welch@ucalgary.ca

ABSTRACT. In this contribution we report on solution processed red OLEDs based upon a N-annulated perylene diimide dimer, namely tPDI₂N-EH, a red-light emitting molecule. OLED devices with the architecture of glass/ITO/PEDOT:PSS/EML/LiF/Ag (EML = emitting layer) were fabricated with EMLs comprised of tPDI₂N-EH neat and blended with poly (9,9-dicofluorene, PFO), all solution processed from non-halogenated solvents. The photophysical and electrophysical performance of PFO:tPDI₂N-EH-blend films with different composition ratios were investigated. The PFO:tPDI₂N-EH-based OLEDs with a 2:18 ratio exhibited best performance. The PFO:tPDI₂N-EH-based OLEDs gave red electroluminescence with the emission

wavelength of 635 nm and the CIE (international commission on illumination) coordinates of ($x = 0.672$, $y = 0.321$). OLEDs with EMLs fabricated using roll-to-roll compatible methods are also demonstrated.

KEYWORDS: organic light emitting diode, solution processing, slot-die coating, organic dyes, perylene diimide, N-annulation

1. Introduction

Organic light-emitting diodes (OLEDs) have successfully been deployed in light fixtures, mobile phones, and televisions over the past few years owing to continued improvements in both performance and lifetimes¹⁻⁵. OLEDs are multilayer devices with each layer having a distinct function such as charge-injection, charge-transport, and light emission. The active emissive layer (EML) dictates the colour and maximum efficiency of OLEDs. For solution processing of electronically active layers; spin-coating⁶, roll-to-roll coating⁷ and inkjet printing⁸ are the most common methods used. Solution processing is more challenging than thermal evaporation due to difficulties in forming distinct layers one on top of each other without bleeding or swelling. Recently, it has been shown that solution processed OLEDs can match the performance of thermally evaporated OLEDs⁹. To create high-performance solution-processed OLEDs both conjugated polymers¹⁰ and small molecules¹¹ have been used as the core component of the EML.

To date the efficiency and purity of red colour solution processed OLEDs remains behind that of other coloured OLEDs (i.e. blue, green and orange)¹². This is primarily a result of low-energy fluorescence being competitive with non-radiative decay pathways¹³. Most highly efficient red-emitting materials are organometallic in nature¹⁴ and suffer from high costs and poor

environmental stability. The design of new metal-free organic small molecules is a viable route towards low-cost, high-performance, large area red OLEDs.

The perylene diimide (PDI) chromophore is one of the best candidates to construct new emitters for solution-processed red OLEDs owing to a pure red colour, high quantum yield photoluminescence, and high thermal and photochemical stability¹⁵⁻¹⁷. Furthermore, PDIs can be rendered soluble in a range of solvents and thus are suitable for large area roll-to-roll coating¹⁸⁻²⁰. PDI-based materials have found wide utility as active materials in transistors^{21,22}, solar cells^{23,24} and OLEDs²⁵⁻²⁷. PDI-based OLEDs typically have pure deep red electroluminescence with the emission wavelength of 690 nm and CIE coordinates of (x = 0.69, y = 0.29)²⁵. Recently, stable red emission from a PDI-based OLED with external quantum efficiency of 4.93% was reported²⁸.

Here, we report red OLEDs based on an emissive dimeric PDI, namely tPDI₂N-EH. This compound is a N-annulated PDI dimer that has found utility as a non-fullerene acceptor for organic photovoltaics²⁹. Blending tPDI₂N-EH with polyfluorene based polymers and used as the EML lead to high-performance OLED devices. The optical and electrophysical properties of PFO:tPDI₂N-EH blended films were studied. The best PFO:tPDI₂N-EH blend OLEDs were compared with high-performance PFO and poly[(9,9-di-n-octylfluorenyl-2,7-diyl)-alt-(benzo[2,1,3]thiadiazol-4,8-diyl)] (F8BT) blend films. Best devices were fabricated by slot-die coating, a roll-to-roll compatible method, as proof-of-concept.

2. Results and Discussion

2.1 Materials Selection

The N-annulated PDI dimer, tPDI₂N-EH (Figure 1a)²⁹, can be synthesized on multi-gram scale, is semiconducting, and can be coated via roll-to-roll processes from non-halogenated solvents^{18,19}. It has a red luminescence peak at 650 nm (Figure 1b) and is chemically stable as a film in light.

Thus, this material is appropriate for use as a solution processable light emitter. The luminescent conjugated polymers PFO and poly(9,9-dioctylfluorene-alt-benzothiadiazole) (F8BT) (structures are shown in Figure 1a) were selected as a hole transporter and control emitter, respectively, since they exhibit high light stability³⁰ and consistent performance as light emitters in OLEDs³¹⁻³⁴. A recent report has shown that PFO:F8BT-ink formulations are suitable to be slot-die coated into a OLED structure³⁵. PFO:F8BT based OLEDs were fabricated as control devices. The PFO polymer is p-type with appropriate electronic energy levels to pair with the F8BT or tPDI₂N-EH to facilitate hole transport (Figure 1c). Moreover, the wavelengths of the tPDI₂N-EH absorption and PFO luminescence overlap (Figure 1b) enabling Förster Resonance Energy Transfer (FRET) to occur from PFO to tPDI₂N-EH. This makes the PFO:tPDI₂N-EH system an excellent candidate as a OLED EML.

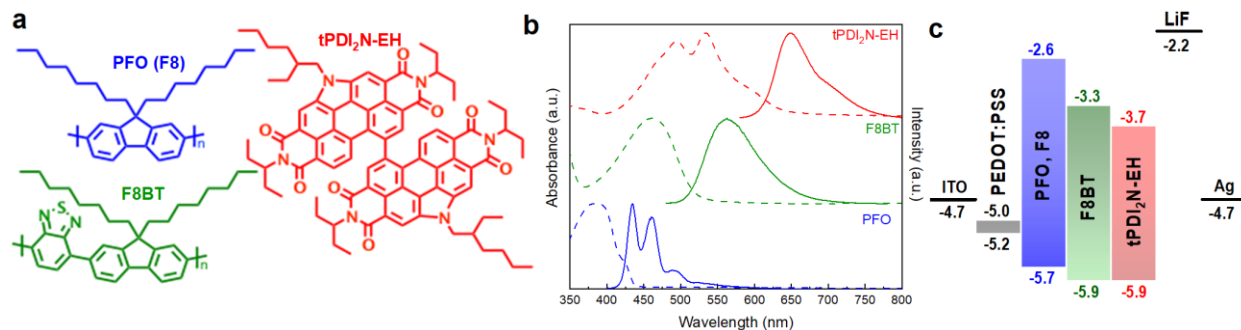


Figure 1. (a) Chemical structures of the polymers PFO (F8) and F8BT, and the small molecule tPDI₂N-EH used in this study. (b) Normalized absorption and photoluminescence spectra of PFO (blue dash and solid line), F8BT (green dash and solid line), and tPDI₂N-EH (red dash and solid line) films spin-cast from toluene at 15 mg mL⁻¹ under $\lambda_{\text{ex}} = 350$ nm, 400 nm and 530 nm, respectively. (c) Energy level diagram with values for organic materials (energy levels taken from the relevant literature, the PEDOT:PSS has a work function of 5.0 - 5.2 eV).

2.2 OLEDs - Spin-coated devices

Device Fabrication and Characterization

OLED devices with the structure of glass/ITO/PEDOT:PSS/EML/LiF/Ag were fabricated and tested at ambient condition. Control devices with an EML of PFO:F8BT-blend film were spin-cast from toluene with the ratio of 19:1 at 15 mg ml⁻¹. EMLs comprised of PFO:tPDI₂N-EH-blend films were spin-cast from toluene at different ratios (from 19:1 to 1:19). The full details of the fabrication technique can be found in the electronic supplementary material (ESI). Electrical characterization of the devices was performed with a Keithley 2612B source-meter combined with the calibrated Si-photodiode and spectrometer.

Photophysical properties of the PFO:tPDI₂N-EH films

The optical absorption and photoluminescence (PL) spectra of PFO:tPDI₂N-EH-blend films are shown in Figure 2. The absorption band from 330 nm to 430 nm is attributed to PFO and from 450 nm to 650 nm is attributed to tPDI₂N-EH. Changing the ratio from 19:1 to 1:19 (PFO:tPDI₂N-EH) results in an expected decrease/increase of the PFO/tPDI₂N-EH absorption bands with no significant changes in shape or position of each spectrum (Figure 2a).

Excitation at 400 nm (near peak absorption of PFO) of blended films with the ratios of 19:1 and 18:2 yields spectra with quenched emission of PFO (from 430-500 nm) and longer wave emission from 600-750 nm which is attributed with tPDI₂N-EH. The quenched PL of PFO is associated with FRET from PFO to tPDI₂N-EH. Increasing the concentration of tPDI₂N-EH in blend films leads to complete quenching of the PFO light emission (at a ratio from 15:5 to 1:19) and increased PL of tPDI₂N-EH compared to neat film (Figure 2b)

Excitation at 530 nm of blended films results in only one emission band from 600-750 nm, a result of PL from tPDI₂N-EH (Figure 2c). When compared to PL of a neat tPDI₂N-EH film, there is an increase in PL intensity of tPDI₂N-EH films with addition of PFO. This is associated with

exciton localization within the tPDI₂N-EH domains caused by the PFO energy barriers of PFO (Figure 1c). Note, the red-shift in PL spectra of tPDI₂N-EH (from 630 nm to 650 nm) with increasing tPDI₂N-EH concentration is the result of aggregation of the tPDI₂N-EH molecules. Thus, the PFO:tPDI₂N-EH-blend films with ratio from 1:19 to 10:10 (highest PL intensity) appears optimum for utilization in OLEDs.

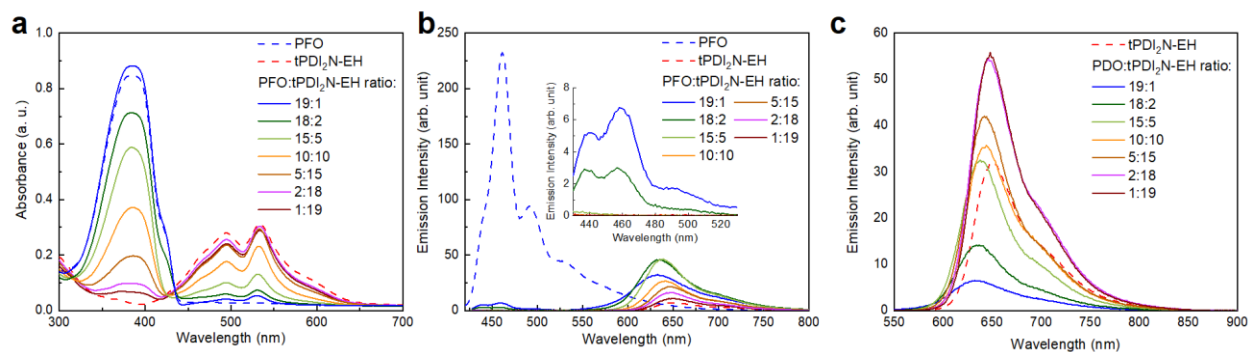


Figure 2. (a) Optical absorption and (b, c) photoluminescence spectra of PFO:tPDI₂N-EH-blend and neat films spin-cast from toluene at 15 mg mL⁻¹ under (b) λ_{ex} = 400 nm and (c) 530 nm.

Table 1. Optical properties of tPDI₂N-EH and PFO:tPDI₂N-EH-blend films.

Compounds	PFO:tPDI ₂ N-EH ratio	Emission of tPDI ₂ N-EH			
		under λ_{ex} = 400 nm		under λ_{ex} = 530 nm	
		max	FWHM ¹	max	FWHM ¹
PFO:tPDI ₂ N-EH	19:1	633	77	633	75
PFO:tPDI ₂ N-EH	18:2	635	63	636	62
PFO:tPDI ₂ N-EH	15:5	639	55	638	55
PFO:tPDI ₂ N-EH	10:10	641	57	642	57
PFO:tPDI ₂ N-EH	5:15	645	54	644	55
PFO:tPDI ₂ N-EH	2:18	646	57	647	60
PFO:tPDI ₂ N-EH	1:19	648	56	647	57
tPDI ₂ N-EH ²	-	653	60	650	60

¹FWHM - full width at half maximum; tPDI₂N-EH and PFO:tPDI₂N-EH-blend films was spin-cast on glass from toluene at 15 mg mL⁻¹.

²Quantum yield photoluminescence of tPDI₂N-EH film of 16%.

OLED device characteristics based on tPDI₂N-EH and PFO:tPDI₂N-EH-blend films with different ratios are shown in Figure 3 and Table 2; the data include graphics of current density-voltage curves (J-V, Figure 3a), luminance versus applied voltage curves (L-V, Figure 3b) and luminous efficiency versus current density curves (LE-J, Figure 3c). The OLEDs based on only tPDI₂N-EH films as the EML showed a maximum luminous efficiency (LE) of around 4×10^{-3} cd A⁻¹ with a maximum brightness of 4.1 cd m⁻², which agree well with the previously obtained data for other PDI-based OLEDs²⁵. The highest performance OLEDs were based on PFO:tPDI₂N-EH EML with the blend ratio of 2:18 and had the maximum LE of 0.05 cd A⁻¹, power efficiency (PE) of 0.03 lm W⁻¹, and external quantum efficiency (EQE) of 0.06%. Increasing the concentration of PFO in PFO:tPDI₂N-EH-blend leads to performance deterioration of the fabricated OLEDs, which agrees well with the PL data (Figure S1). The turn-on voltage of the tPDI₂N-EH-based OLEDs decreases when PFO is added to the EML. Adding the PFO, which has a higher lying HOMO energy level than tPDI₂N-EH, helps facilitate hole injection from PEDOT:PSS to the EML. The turn-on voltage of 2.6 V for the OLEDs with PFO:tPDI₂N-EH EMLs is the lowest reported for PDI-based OLEDs^{25,26,28,36}.

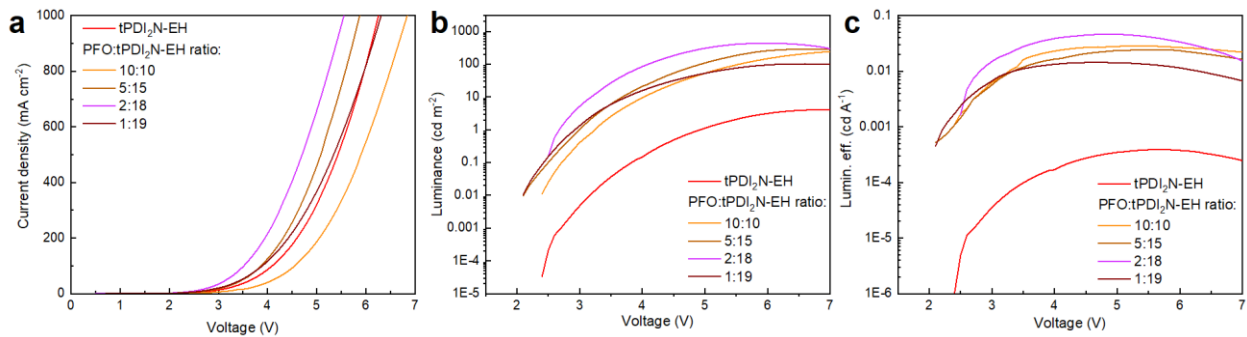


Figure 3. (a) Current density-voltage (J - V) characteristics, (b) luminance versus applied voltage (L - V , cd m⁻²) and (c) luminous efficiency (lumin. eff.) versus current density (LE - J , cd A⁻¹) of PFO:tPDI₂N-EH OLEDs at selected ratios.

Table 2. Summary of device performance for OLEDs based on tPDI₂N-EH and PFO:tPDI₂N-EH- blend films with different ratio spin-coated on the glass.

Emitting layer	ratio ¹	V_{on} [V] ²	EQE_{max} [%] ³	LE_{max} [cd A ⁻¹] ⁴	PE_{max} [lm W ⁻¹] ⁵	L_{max} [cd m ⁻²] ⁶
tPDI ₂ N-EH	-	4.9	0.000504	0.000392	0.000236	4.1
PFO: tPDI ₂ N-EH	10:10	3.2	0.035	0.028	0.019	262.3
PFO: tPDI ₂ N-EH	5:15	3.0	0.031	0.025	0.015	288.5
PFO: tPDI ₂ N-EH	2:18	2.6	0.057	0.046	0.031	435.4
PFO: tPDI ₂ N-EH	1:19	2.7	0.018	0.014	0.010	101.8

¹PFO:tPDI₂N-EH ratio

²Turn on voltage was determined at the brightness of 1 cd m⁻²

³EQE - external quantum efficiency

⁴LE - luminous efficiency

⁵PE - power efficiency

⁶ L_{max} - maximum of luminous

OLED Electroluminescence

The electroluminescence (EL), CIE, and current-voltage-luminance characteristics of PFO:F8BT (19:1 ratio) and optimized PFO:tPDI₂N-EH-based (2:18 ratio) OLEDs are shown in Figure 4 and Table 3. PFO:F8BT-based OLEDs demonstrated the maximum LE of 1.24 cd A⁻¹, PE of 0.4 lm W⁻¹ and brightness of 1950 cd m⁻² with white-green spectrum at maximum of 530 nm, full width at half maximum (FWHM) of 105nm, and CIE coordinates located at (x, y) = (0.383, y = 0.514). This data is well aligned with literature^{32,35}. Using tPDI₂N-EH instead of F8BT with PFO shifts the EL to red, which agrees well with the PL of tPDI₂N-EH. The PFO:tPDI₂N-EH-based OLEDs exhibit a narrow peak of EL with the maximum emission at 635 nm and FWHM of 60 nm with the CIE coordinates of (x, y) = (0.672, 0.321). Moreover, using tPDI₂N-EH decreases the turn-on voltage to 2.6 V due to the lower LUMO energy level and easy injection of electrons from the contacts to the active layer.

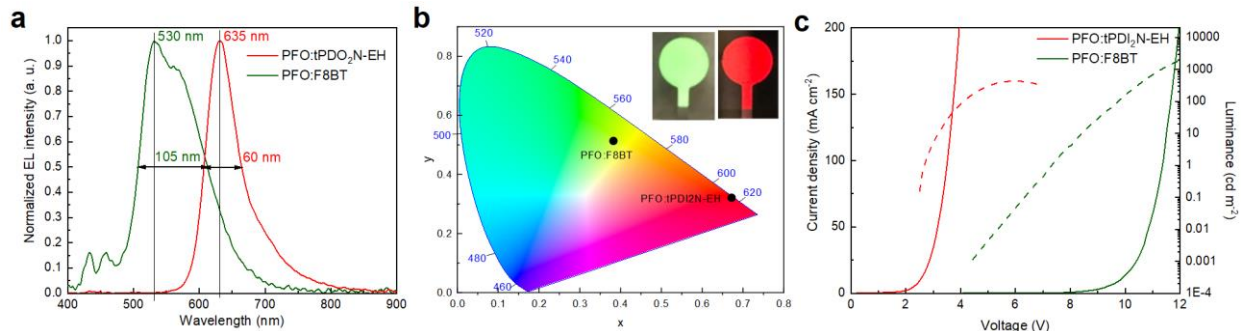


Figure 4. (a) Normalized electroluminescence (EL) and (b) color coordinates spectra, (c) current-voltage-luminance characteristics of PFO:F8BT (ratio 19:1) and PFO:tPDI₂N-EH (ratio 2:18) blends.

Table 3. Summary of device performance for OLEDs based on PFO:F8BT and PFO:tPDI₂N-EH- blend films spin-coated on glass.

Emitting layer	ratio ¹	V_{on} [V] ²	EQE_{max} [%] ³	LE_{max} [cd A ⁻¹] ⁴	PE_{max} [lm W ⁻¹] ⁵	L_{max} [cd m ⁻²] ⁶
PFO:F8BT	19:1	7.3	0.406	1.24	0.376	1951.6
PFO:tPDI ₂ N-EH	2:18	2.6	0.057	0.046	0.031	435.4

¹PFO:F8BT or PFO:tPDI₂N-EH ratio

²Turn on voltage was determined at the brightness of 1 cd m⁻²

³EQE - external quantum efficiency

⁴LE - luminous efficiency

⁵PE - power efficiency

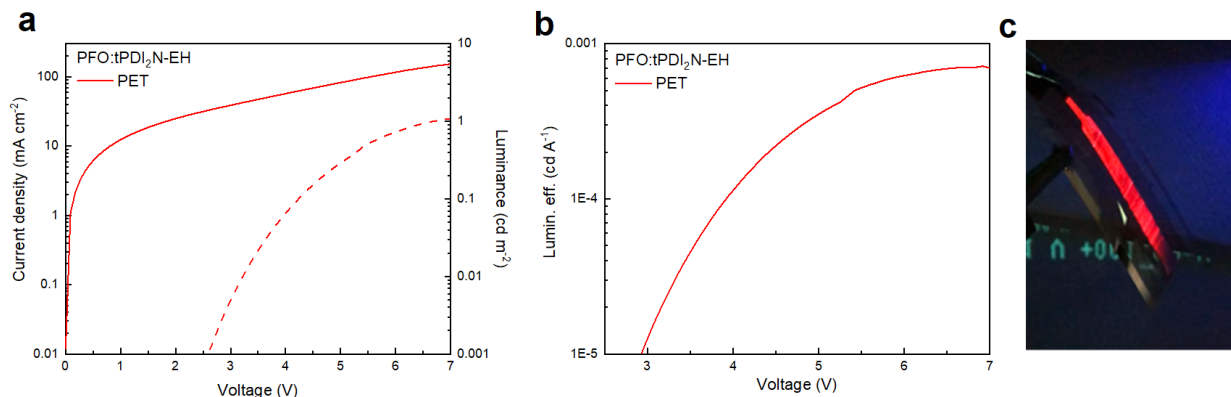
⁶ L_{max} - maximum of luminous

2.3 OLEDs - slot-die coated devices

The roll-to-roll compatibility of organic and inorganic layers of OLED devices is an important consideration for large-scale fabrication methods⁷. Thus, we aimed to repeat our best spin-coated devices with a slot-die coating technique. A FOM Nano Roll Coater (slot-die head with 13 mm shim width) was used to coat both the PEDOT:PSS interlayer and PFO:tPDI₂N-EH (2:18) EML onto a PET/ITO substrate/anode base. The PEDOT:PSS interlayer was slot-die coated with the

coating speed of 0.1 mm^{-1} , dispensing rate of $12 \text{ } \mu\text{L min}^{-1}$, and substrate temperature of $50 \text{ }^\circ\text{C}$. The layer was thermally annealed at $100 \text{ }^\circ\text{C}$ for 15 min prior to the deposition of the EML. The PFO:tPDI₂N-EH (2:18) solutions were coated from toluene at 30 mg mL^{-1} with the coating speed of 0.3 mm^{-1} , dispensing rate of $30 \text{ } \mu\text{L min}^{-1}$ at room temperature. The films were then dried in air at $100 \text{ }^\circ\text{C}$ for 30 minutes. A LiF/Ag electrode was thermally deposited using a thermal evaporation system through a shadow mask under a base pressure of $\sim 2 \times 10^{-6}$ torr (this top electrode was used for consistency in comparing to the spin-coated OLEDs). The device area was 160 mm^2 as defined by the overlapping area of the ITO films and top electrodes. The optical absorption spectra of the roll-to-roll coated devices (in comparison to the spin-coated ones) can be found in the ESI (Figure S2).

The current-voltage-luminance characteristics and *LE* versus current density of OLED devices with the PEDOT:PSS and PFO:tPDI₂N-EH layers roll-to-roll coated on PET are shown in Figure 5 and electrophysical parameters are summarized in Table 4. The OLEDs had a turn-on voltage of 6.6 V and maximum brightness of 1.1 cd m^{-2} , demonstrating a fully functioning large area, roll-to-roll compatible coated device. Thus, this work shows that large-area OLEDs can be fabricated using slot-die coating techniques. The synthesis of new PDIs with high quantum yield and narrow peak luminescence of films, and optimized roll-to-roll coating of OLED layers is a viable pathway towards developing high-performance OLEDs for large-scale manufacturing.



Films 5. (a) Current-voltage-luminance characteristics and (b) luminous efficiency (lumin. eff.) versus current density ($LE-J$, $cd A^{-1}$) of PFO:tPDI₂N-EH roll-to-roll coated on PET. (c) Photo of electroluminescent of PFO:tPDI₂N-EH OLEDs on PET.

Table 4. Summary of device performance for spin-cast and slot-die coating OLEDs based on PFO:tPDI₂N-EH-blend films.

Emitting layer	substrate	V_{on} [V] ²	EQE_{max} [%] ³	LE_{max} [$cd A^{-1}$] ⁴	PE_{max} [$lm W^{-1}$] ⁵	L_{max} [$cd m^{-2}$] ⁶
PFO: tPDI ₂ N-EH ¹	PET/ITO ⁷	6.6	0.000147	0.000718	0.000054	1.1

¹PFO:tPDI₂N-EH ratio is 2:18
²Turn on voltage was determined at the brightness of 1 $cd m^{-2}$
³EQE - external quantum efficiency
⁴LE - luminous efficiency
⁵PE - power efficiency
⁶ L_{max} - maximum of luminous
⁷The EML prepared from a solvent of toluene by roll-to-roll coated with active are 160 mm^2

Conclusion

We have presented electrically pumped, solution processed red OLEDs based on a N-annulated perylene diimide dimer as the emitting material. Use of the polyfluorene based polymer PFO as an additive for the red-emitter tPDI₂N-EH resulted in large performance boosts with an optimal PFO:tPDI₂N-EH ratio of 2:18 identified. The best efficiencies of PFO:tPDI₂N-EH-based OLEDs exhibited a maximum LE of 0.05 $cd A^{-1}$, power efficiency (PE) of 0.03 $lm W^{-1}$ and external quantum efficiency (EQE) of 0.06%, and are among the best for PDI-based OLEDs. Proof-of-concept large-scale fabrication of OLEDs was demonstrated by roll-to-roll compatible coating of both the PEDOT:PSS hole injection layer and PFO:tPDI₂N-EH emitting layer of OLEDs with large area (160 mm^2) on plastic substrates. This work highlights the potential of N-annulated perylene diimide based materials to deliver commercially relevant advanced lighting devices.

Acknowledgement

GCW acknowledges CFI JELF (34102), CRC, WED, and the University of Calgary. SVD is grateful for a MITACS fellowship. Authors would like to thank GenOptic LED Inc. for their financial support.

References

- (1) Chen, H.-W.; Lee, J.-H.; Lin, B.-Y.; Chen, S.; Wu, S.-T. Liquid Crystal Display and Organic Light-Emitting Diode Display: Present Status and Future Perspectives. *Light Sci. Appl.* **2018**, *7* (3), 17168–17168. <https://doi.org/10.1038/lsa.2017.168>.
- (2) Ràfols-Ribé, J.; Will, P.-A.; Hänisch, C.; Gonzalez-Silveira, M.; Lenk, S.; Rodríguez-Viejo, J.; Reineke, S. High-Performance Organic Light-Emitting Diodes Comprising Ultrastable Glass Layers. *Sci. Adv.* **2018**, *4* (5), eaar8332. <https://doi.org/10.1126/sciadv.aar8332>.
- (3) Kotadiya, N. B.; Blom, P. W. M.; Wetzelaer, G.-J. A. H. Efficient and Stable Single-Layer Organic Light-Emitting Diodes Based on Thermally Activated Delayed Fluorescence. *Nat. Photonics* **2019**. <https://doi.org/10.1038/s41566-019-0488-1>.
- (4) Guo, K.; Wang, H.; Wang, Z.; Si, C.; Peng, C.; Chen, G.; Zhang, J.; Wang, G.; Wei, B. Stable Green Phosphorescence Organic Light-Emitting Diodes with Low Efficiency Roll-off Using a Novel Bipolar Thermally Activated Delayed Fluorescence Material as Host. *Chem. Sci.* **2017**, *8* (2), 1259–1268. <https://doi.org/10.1039/C6SC03008D>.
- (5) Sato, S.; Ohisa, S.; Hayashi, Y.; Sato, R.; Yokoyama, D.; Kato, T.; Suzuki, M.; Chiba, T.; Pu, Y.; Kido, J. Air-Stable and High-Performance Solution-Processed Organic Light-Emitting Devices Based on Hydrophobic Polymeric Ionic Liquid Carrier-Injection Layers. *Adv. Mater.* **2018**, *30* (18), 1705915. <https://doi.org/10.1002/adma.201705915>.

- (6) Lee, B. R.; Jung, E. D.; Park, J. S.; Nam, Y. S.; Min, S. H.; Kim, B.-S.; Lee, K.-M.; Jeong, J.-R.; Friend, R. H.; Kim, J.-S.; et al. Highly Efficient Inverted Polymer Light-Emitting Diodes Using Surface Modifications of ZnO Layer. *Nat. Commun.* **2014**, *5* (1), 4840. <https://doi.org/10.1038/ncomms5840>.
- (7) Sandström, A.; Dam, H. F.; Krebs, F. C.; Edman, L. Ambient Fabrication of Flexible and Large-Area Organic Light-Emitting Devices Using Slot-Die Coating. *Nat. Commun.* **2012**, *3* (1), 1002. <https://doi.org/10.1038/ncomms2002>.
- (8) C, A.; Szymański, M. Z.; Łuszczynska, B.; Ulański, J. Inkjet Printing of Super Yellow: Ink Formulation, Film Optimization, OLEDs Fabrication, and Transient Electroluminescence. *Sci. Rep.* **2019**, *9* (1), 8493. <https://doi.org/10.1038/s41598-019-44824-w>.
- (9) Sree, V. G.; Park, H.; Cho, W.; Jin, S.-H. High Efficient Vacuum Deposited Red Organic Light-Emitting Diodes Compared with Their Solution-Processed Counterpart. *Mol. Cryst. Liq. Cryst.* **2017**, *654* (1), 73–82. <https://doi.org/10.1080/15421406.2017.1355696>.
- (10) Burns, S.; MacLeod, J.; Trang Do, T.; Sonar, P.; Yambem, S. D. Effect of Thermal Annealing Super Yellow Emissive Layer on Efficiency of OLEDs. *Sci. Rep.* **2017**, *7* (1), 40805. <https://doi.org/10.1038/srep40805>.
- (11) Aizawa, N.; Pu, Y.-J.; Watanabe, M.; Chiba, T.; Ideta, K.; Toyota, N.; Igarashi, M.; Suzuri, Y.; Sasabe, H.; Kido, J. Solution-Processed Multilayer Small-Molecule Light-Emitting Devices with High-Efficiency White-Light Emission. *Nat. Commun.* **2014**, *5* (1), 5756. <https://doi.org/10.1038/ncomms6756>.
- (12) Wei, Q.; Fei, N.; Islam, A.; Lei, T.; Hong, L.; Peng, R.; Fan, X.; Chen, L.; Gao, P.; Ge, Z.

- Small-Molecule Emitters with High Quantum Efficiency: Mechanisms, Structures, and Applications in OLED Devices. *Adv. Opt. Mater.* **2018**, *6* (20), 1800512. <https://doi.org/10.1002/adom.201800512>.
- (13) Zhang, Q.; Kuwabara, H.; Potscavage, W. J.; Huang, S.; Hatae, Y.; Shibata, T.; Adachi, C. Anthraquinone-Based Intramolecular Charge-Transfer Compounds: Computational Molecular Design, Thermally Activated Delayed Fluorescence, and Highly Efficient Red Electroluminescence. *J. Am. Chem. Soc.* **2014**, *136* (52), 18070–18081. <https://doi.org/10.1021/ja510144h>.
- (14) Xiang, H.; Cheng, J.; Ma, X.; Zhou, X.; Chruma, J. J. Near-Infrared Phosphorescence: Materials and Applications. *Chem. Soc. Rev.* **2013**, *42* (14), 6128. <https://doi.org/10.1039/c3cs60029g>.
- (15) Schmidt, D.; Stolte, M.; Süß, J.; Liess, A.; Stepanenko, V.; Würthner, F. Protein-like Enwrapped Perylene Bisimide Chromophore as a Bright Microcrystalline Emitter Material. *Angew. Chemie Int. Ed.* **2019**, *58* (38), 13385–13389. <https://doi.org/10.1002/anie.201907618>.
- (16) Sabatini, R. P.; Zhang, B.; Gupta, A.; Leoni, J.; Wong, W. W. H.; Lakhwani, G. Molecularly Isolated Perylene Diimides Enable Both Strong Exciton–Photon Coupling and High Photoluminescence Quantum Yield. *J. Mater. Chem. C* **2019**, *7* (10), 2954–2960. <https://doi.org/10.1039/C9TC00093C>.
- (17) Zhang, B.; Soleimaninejad, H.; Jones, D. J.; White, J. M.; Ghiggino, K. P.; Smith, T. A.; Wong, W. W. H. Highly Fluorescent Molecularly Insulated Perylene Diimides: Effect of Concentration on Photophysical Properties. *Chem. Mater.* **2017**, *29* (19), 8395–8403.

<https://doi.org/10.1021/acs.chemmater.7b02968>.

- (18) Laventure, A.; Harding, C. R.; Cieplechowicz, E.; Li, Z.; Wang, J.; Zou, Y.; Welch, G. C. Screening Quinoxaline-Type Donor Polymers for Roll-to-Roll Processing Compatible Organic Photovoltaics. *ACS Appl. Polym. Mater.* **2019**, *acsapm.9b00433*. <https://doi.org/10.1021/acsapm.9b00433>.
- (19) Tintori, F.; Laventure, A.; Welch, G. C. Perylene Diimide Based Organic Photovoltaics with Slot-Die Coated Active Layers from Halogen-Free Solvents in Air at Room Temperature. *ACS Appl. Mater. Interfaces* **2019**, *acsami.9b14251*. <https://doi.org/10.1021/acsami.9b14251>.
- (20) Laventure, A.; Stanzel, S.; Payne, A.-J.; Lessard, B. H.; Welch, G. C. A Ring Fused N-Annulated PDI Non-Fullerene Acceptor for High Open Circuit Voltage Solar Cells Processed from Non-Halogenated Solvents. *Synth. Met.* **2019**, *250*, 55–62. <https://doi.org/10.1016/j.synthmet.2019.02.010>.
- (21) Gupta, R. K.; Dey, A.; Singh, A.; Iyer, P. K.; Sudhakar, A. A. Heteroatom Bay-Annulated Perylene Bisimides: New Materials for Organic Field Effect Transistors. *ACS Appl. Electron. Mater.* **2019**, *1* (8), 1378–1386. <https://doi.org/10.1021/acsaelm.9b00004>.
- (22) Li, G.; Li, D.; Liu, X.; Xu, H.; Zhang, J.; Wang, S.; Liu, Z.; Tang, B. Novel Dithiano-Thieno Fused Perylene Diimides: Synthesis, Characterization and Application in Organic Thin-Film Transistors (OTFTs). *Chem. Commun.* **2019**, *55* (65), 9661–9664. <https://doi.org/10.1039/C9CC04133H>.
- (23) Sun, D.; Meng, D.; Cai, Y.; Fan, B.; Li, Y.; Jiang, W.; Huo, L.; Sun, Y.; Wang, Z. Non-

- Fullerene-Acceptor-Based Bulk-Heterojunction Organic Solar Cells with Efficiency over 7%. *J. Am. Chem. Soc.* **2015**, *137* (34), 11156–11162. <https://doi.org/10.1021/jacs.5b06414>.
- (24) Zhang, J.; Li, Y.; Huang, J.; Hu, H.; Zhang, G.; Ma, T.; Chow, P. C. Y.; Ade, H.; Pan, D.; Yan, H. Ring-Fusion of Perylene Diimide Acceptor Enabling Efficient Nonfullerene Organic Solar Cells with a Small Voltage Loss. *J. Am. Chem. Soc.* **2017**, *139* (45), 16092–16095. <https://doi.org/10.1021/jacs.7b09998>.
- (25) Kozma, E.; Mróz, W.; Villafiorita-Monteleone, F.; Galeotti, F.; Andicsová-Eckstein, A.; Catellani, M.; Botta, C. Perylene Diimide Derivatives as Red and Deep Red-Emitters for Fully Solution Processable OLEDs. *RSC Adv.* **2016**, *6* (66), 61175–61179. <https://doi.org/10.1039/C6RA10467C>.
- (26) Li, G.; Zhao, Y.; Li, J.; Cao, J.; Zhu, J.; Sun, X. W.; Zhang, Q. Synthesis, Characterization, Physical Properties, and OLED Application of Single BN-Fused Perylene Diimide. *J. Org. Chem.* **2015**, *80* (1), 196–203. <https://doi.org/10.1021/jo502296z>.
- (27) Matussek, M.; Filapek, M.; Gancarz, P.; Krompiec, S.; Grzegorz Małecki, J.; Kotowicz, S.; Siwy, M.; Maćkowski, S.; Chrobok, A.; Schab-Balcerzak, E.; et al. Synthesis and Photophysical Properties of New Perylene Bisimide Derivatives for Application as Emitting Materials in OLEDs. *Dye. Pigment.* **2018**, *159*, 590–599. <https://doi.org/10.1016/j.dyepig.2018.07.006>.
- (28) Zong, L.; Gong, Y.; Yu, Y.; Xie, Y.; Xie, G.; Peng, Q.; Li, Q.; Li, Z. New Perylene Diimide Derivatives: Stable Red Emission, Adjustable Property from ACQ to AIE, and Good Device Performance with an EQE Value of 4.93%. *Sci. Bull.* **2018**, *63* (2), 108–116. <https://doi.org/10.1016/j.scib.2017.10.021>.

- (29) Dayneko, S. V.; Hendsbee, A. D.; Welch, G. C. Combining Facile Synthetic Methods with Greener Processing for Efficient Polymer-Perylene Diimide Based Organic Solar Cells. *Small Methods* **2018**, *2* (6), 1800081. <https://doi.org/10.1002/smt.201800081>.
- (30) Smirnov, J. R. C.; Sousaraei, A.; Osorio, M. R.; Casado, S.; Hernández, J. J.; Wu, L.; Zhang, Q.; Xia, R.; Granados, D.; Wannemacher, R.; et al. Flexible Distributed Feedback Lasers Based on Nanoimprinted Cellulose Diacetate with Efficient Multiple Wavelength Lasing. *npj Flex. Electron.* **2019**, *3* (1), 17. <https://doi.org/10.1038/s41528-019-0062-4>.
- (31) Ahn, J. H.; Wang, C.; Perepichka, I. F.; Bryce, M. R.; Petty, M. C. Blue Organic Light Emitting Devices with Improved Colour Purity and Efficiency through Blending of Poly(9,9-Dioctyl-2,7-Fluorene) with an Electron Transporting Material. *J. Mater. Chem.* **2007**, *17* (29), 2996. <https://doi.org/10.1039/b700047b>.
- (32) de Azevedo, D.; Freitas, J. N.; Domingues, R. A.; Faleiros, M. M.; Atvars, T. D. Z. Correlation between the PL and EL Emissions of Polyfluorene-Based Diodes Using Bilayers or Polymer Blends. *Synth. Met.* **2017**, *233*, 28–34. <https://doi.org/10.1016/j.synthmet.2017.08.015>.
- (33) Kwak, K.; Cho, K.; Kim, S. Stable Bending Performance of Flexible Organic Light-Emitting Diodes Using IZO Anodes. *Sci. Rep.* **2013**, *3* (1), 2787. <https://doi.org/10.1038/srep02787>.
- (34) Gioti, M.; Kokkinos, D.; Chaidou, C. I.; Laskarakis, A.; Andreopoulou, A. K.; Kallitsis, J. K.; Logothetidis, S. A Comprehensive Study of the Optical Properties of Emitting Polymers for Efficient Flexible OLED Devices. *Phys. status solidi* **2016**, *213* (11), 2947–2953. <https://doi.org/10.1002/pssa.201600651>.

- (35) C, A.; Colella, M.; Griffin, J.; Kingsley, J.; Scarratt, N.; Luszczynska, B.; Ulanski, J. Slot-Die Coating of Double Polymer Layers for the Fabrication of Organic Light Emitting Diodes. *Micromachines* **2019**, *10* (1), 53. <https://doi.org/10.3390/mi10010053>.
- (36) Céspedes-Guirao, F. J.; García-Santamaría, S.; Fernández-Lázaro, F.; Sastre-Santos, A.; Bolink, H. J. Efficient Electroluminescence from a Perylenediimide Fluorophore Obtained from a Simple Solution Processed OLED. *J. Phys. D. Appl. Phys.* **2009**, *42* (10), 105106. <https://doi.org/10.1088/0022-3727/42/10/105106>.

SUPPLEMENT MATERIALS

Red Organic Light-Emitting-Diodes based on a N-Annulated Perylene Diimide Dimer

Sergey V. Dayneko,^a Mohammad Rahmati,^b Majid Pahlevani,^{c,} Gregory C. Welch^{a,*}*

^aDepartment of Chemistry, University of Calgary, 731 Campus Place NW, Calgary, Alberta, Canada T2N 1N4

^bGenoptic LED Inc, 6000 72nd Ave SE, Calgary, AB, Canada, T2C 5B1

^cDepartment of Electrical and Computer Engineering, Queen's University, 19 Union St., Kingston, ON, Canada, K7L 3N6

*E-mail: majid.pahlevani@queensu.ca and gregory.welch@ucalgary.ca

TABLE OF CONTENTS

Materials and Methods	S2
Characteristics of OLEDs.	S4

1. Materials and Methods

Materials: All chemicals/solvents were purchased from Millipore-Sigma and used without further purification. tPDI2N-EH was made as previously reported (Small Methods, 2018, 2, 180081). PFO and F8BT was purchased from Ossila.

UV-Visible Spectroscopy (UV-Vis): All optical absorption measurements were recorded using Agilent Technologies Cary 60 UV-Vis spectrometer at room temperature. Films were spin-cast onto Corning glass micro slides. Prior to use, glass slides were cleaned with soap and water, acetone and isopropanol, and followed by UV/ozone treatment using a Novascan UV/ozone cleaning system.

Atomic Force Microscopy (AFM): AFM measurements were performed by using a TT2- AFM (AFM Workshop) in tapping mode and WSxM software with a resonance frequency of 300 kHz, a force constant of 40 N/m and a reflective back side aluminum coating (Tap300A1-G, BudgetSensors). Samples for AFM measurements were the same ones that were used to collect the respective device parameters.

OLED Device Fabrication and Testing (spin-coated): OLED devices were fabricated on ITO-coated glass substrates (sheet resistance of 10 Ohm Sq⁻¹), which were first cleaned by sequentially ultra-sonicating detergent and de-ionized water, acetone and isopropanol before use. ITO substrates were first pretreated under UV-ozone for 30 minutes. PEDOT:PSS were spin-coated onto the ITO-coated glass substrates at 3,000 rpm for 60s and annealed in air at 120°C.

F8:F8BT:

For deposition of the F8:F8BT active layer, the blend solution of F8:F8BT (ratio 19:1 at total concentration of 15 mg mL⁻¹) dissolved in toluene was spin-cast at 2,000 rpm on top of the PEDOT:PSS layer in air.

F8:tPDI2N-EH:

For deposition of the F8:tPDI2N-EH active layer, the blend solution of F8:tPDI2N-EH (different ratio at total concentration of 15 mg mL⁻¹) dissolved in toluene was spin-cast on top of the PEDOT:PSS layer in air.

Finally, the LiF (1 nm)/Ag (200 nm) electrode was deposited using a thermal evaporation system through a shadow mask under a base pressure of $\sim 2 \times 10^{-6}$ torr. The device area was 9 mm² as defined by the overlapping area of the ITO films and top electrodes.

Current density-voltage (J-V) characteristics were measured using a Keithley 2612B source-meter combined with calibrated Si-photodiode and spectrometer.

2. Characteristics of OLEDs

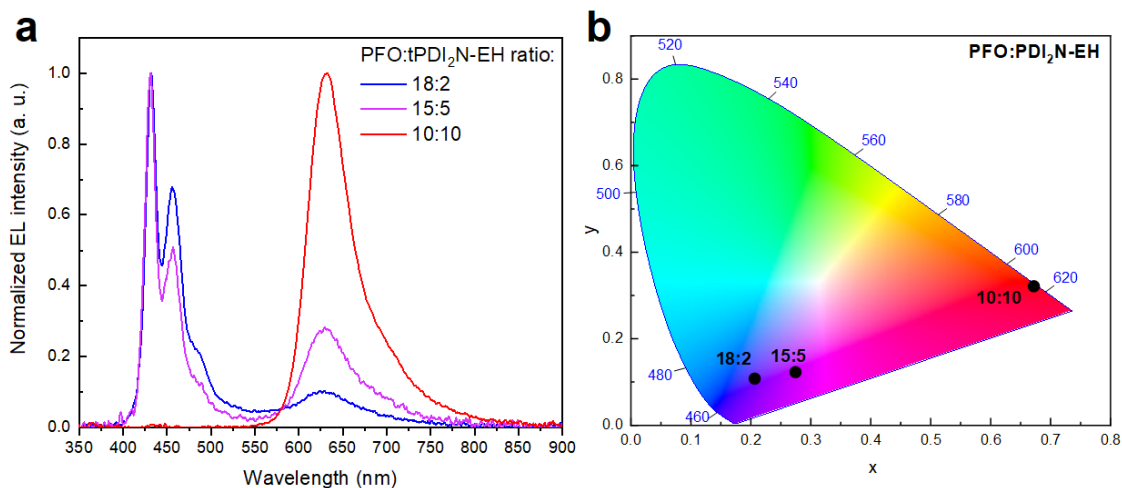


Figure S1. (a) Normalized electroluminescence (EL) and (b) color coordinates spectra of PFO:tPDI₂N-EH-based OLEDs with different ratio of PFO and tPDI₂N-EH.

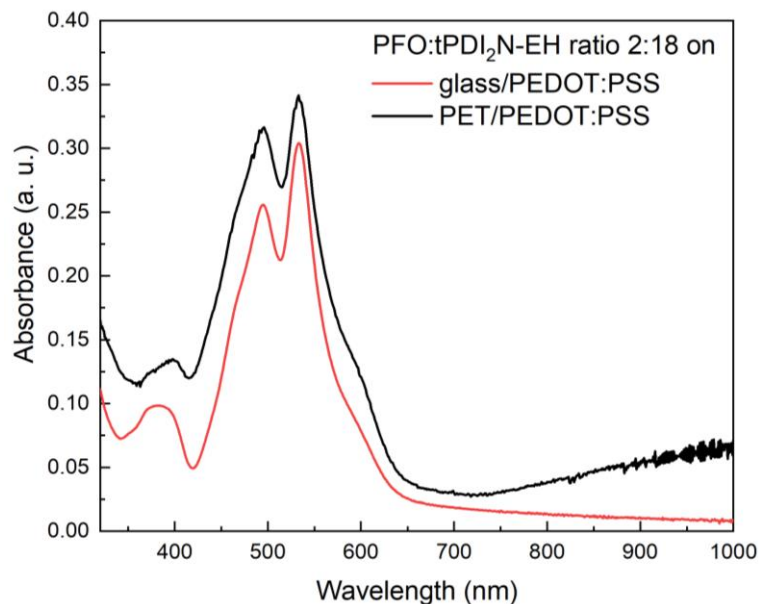


Figure S2. Optical absorption of OLEDs based on PFO:tPDI₂N-EH with ratio of 2:18, spin-cast on glass/ITO/PEDOT:PSS and roll-to-roll coated on PET/ITO/PEDOT:PSS.